ACS Energy LETTERS

http://pubs.acs.org/journal/aelccp

LETTER

In Situ Optical Imaging of Sodium Electrodeposition: Effects of Fluoroethylene Carbonate

Rodrigo Rodriguez,[†] Kathryn E. Loeffler,[†] Sindhu S. Nathan,[†] Jonathan K. Sheavly,[†] Andrei Dolocan,[‡] Adam Heller,[†,∥] and C. Buddie Mullins*[,†,‡,§,∥]

[†]McKetta Department of Chemical Engineering, The University of Texas at Austin, Austin, Texas 78712-1589, United States

[‡]Texas Materials Institute, The University of Texas at Austin, Austin, Texas 78712-1591, United States

[§]Department of Chemistry, The University of Texas at Austin, Austin, Texas 78712-1224, United States

[∥]Center for Electrochemistry, The University of Texas at Austin, Austin Texas 78712-0165, United States

Supporting Information

ABSTRACT: **The morphologies of sodium electrodeposits and gas evolution were studied in a system comprising a symmetrical Na/Na optical cell, a digital microscope, and an electrochemical workstation. Sodium deposition in ethylene carbonate (EC), diethyl carbonate (DEC), and propylene carbonate (PC) generated large volumes of gas and fragile, porous dendrites. The use of fluoroethylene carbonate (FEC) greatly reduced gassing during deposition and demonstrated superior cycling performance, impedance, and cycling efficiency when it was used as a cosolvent with DEC (1:1 vol); however, porous depositions persisted. Time of flight secondary-ion mass spectrometry revealed that the solid-electrolyte interphase formed in FEC/DEC, in contrast with the EC/DEC electrolyte, is thicker, richer in NaF, and forms a less dense polymer organic layer.**

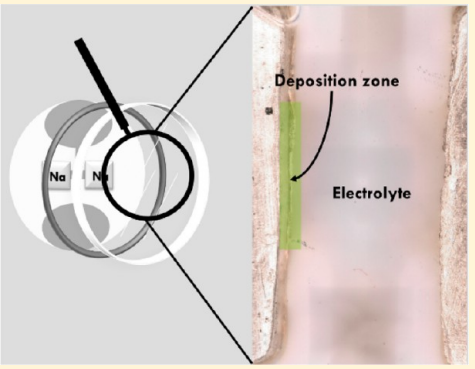

The solid-electrolyte interphase (SEI) affects the morphology and the gassing in the electrodeposition of reactive metals, including the alkali metals.[1−4] The alkali metals reduce the electrolyte to form an SEI surface film that is electronically insulating and ionically conductive.[5] If the SEI layer is stable, it will protect the alkali metal from further parasitic reactions with the electrolyte.[6] When sodium metal is immersed in an organic electrolyte, the SEI grows until electron transport slows sufficiently to hinder further parasitic reactions.[5] SEI thickness, composition, and uniformity are largely dependent on the electrolyte makeup, which also influences sodium deposition morphologies.[5−7] Diffusion of cations through mediums of varying thickness and dissimilar ionic conductivity leads to nonuniform nucleation density and thus a higher propensity for dendrite formation.[7,8]

Akin to lithium metal, sodium metal deposits in dendritic structures with the potential to cause electrical shorting.[3] However, studies on sodium dendrite nucleation, propagation, and mitigation strategies remain, for the most part, unreported.[9,3] Sodium-ion battery (SIB) electrode analogs of lithium-ion batteries typically show inferior performance compared to lithium because of differences in solvation energies, solid-state diffusion, and surface passivation.[10] Considering that dendritic growth on sodium is more severe than on lithium, the development of an electrochemically inactive, porous sodium layer may be a large contributor to poor (SIB) performance as well.[10]

In order to advance SIB technologies, it is essential to understand sodium electrodeposition when sodium is used as an electrode. Although there are many optical studies of lithium deposition−dissolution,[11−15] similar studies of sodium are rare. To the best of our knowledge, there exist only two papers that optically study the formation of sodium dendrites. There is one report of sodium metal cycling in a propylene carbonate (PC) electrolyte at a small rate of 50 μA cm^{-2} where needlelike growth and formation of gas is observed.[3] Another study compares the sodium metal dendrites formed in ethylene carbonate (EC)/PC with and without a polymer additive.[16] However, the effect of charge rate and electrolyte composition, especially the commonly used solvent fluoroethylene carbonate (FEC), on the sodium deposition morphology is still poorly understood.

Here we image in situ the sodium deposition in a home-built, hermetically sealed optical cell[17] (Figures S1 and S2) coupled

Received: June 9, 2017
Accepted: August 15, 2017

DOI: 10.1021/acsenergylett.7b00500
ACS Energy Lett. 2017, 2, 2051−2057

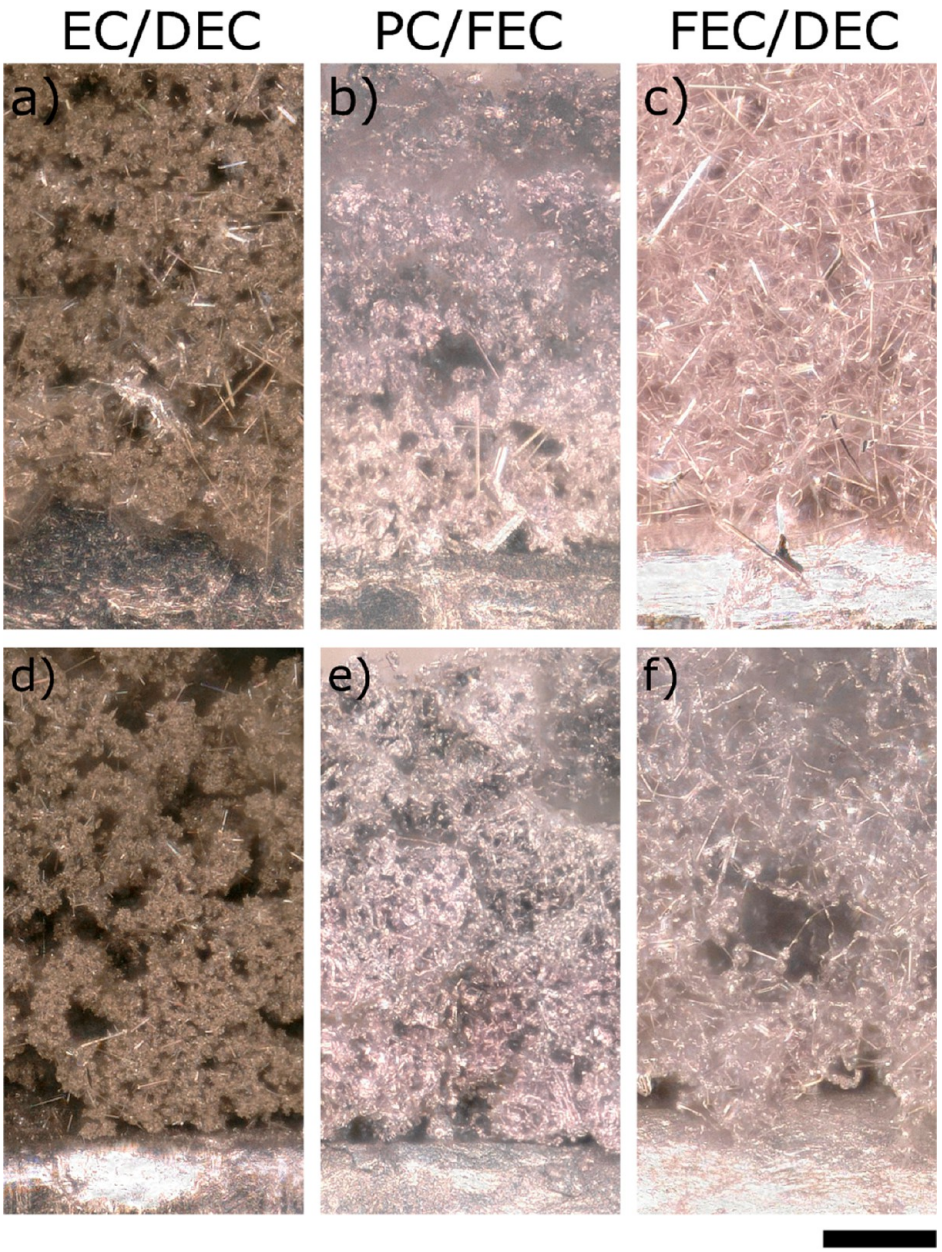

Figure 1. Morphologies of sodium deposited from 1 M $NaPF_6$ in EC/DEC (a, d), PC/FEC (b, e), and FEC/DEC (c, f) upon passage of 4 mAh cm^{-2} at 1 mA cm^{-2} (top images) and 5 mA cm^{-2} (bottom images). Sodium substrates are at the bottom of all images. Entire electrodes, before and after deposition, are shown in Figure S3. Scale bar is 100 μm.

with a high-resolution, Keyence VHX-5000 digital microscope. We compare three electrolytes utilizing frequently used SIB solvents: 1 M NaPF6 in (i) EC/diethyl carbonate (DEC) (1:1 v/v), (ii) PC/FEC (98:2 v/v), and (iii) FEC/DEC (1:1 v/v).[18−20] Optical cell depositions and coin cell cycling data are performed at 1 mA cm^{-2} and 5 mA cm^{-2}. From the optical imaging, we observe formation of porous depositions with varying morphologies. Excessive gas evolution and loss of sodium into the electrolyte (dead sodium) was mitigated when FEC was used as a cosolvent with DEC. Symmetrical coin cell cycling, cycling efficiencies, and electrochemical impedance spectroscopy (EIS) data also corroborate the positive role of the FEC on sodium cyclability. Time of flight secondary-ion mass spectrometry (ToF-SIMS) depth profiling shows that FEC/DEC electrolyte, in contrast with the EC/DEC, forms a NaF-enriched and organic polymer-depleted SEI layer.

Figure 1 shows the solvent dependence of the morphology of the sodium electrodeposited upon passage of 4 mAh cm^{-2}; this quantity of charge formed easily observable dendrites for imaging in the optical cell. All deposits are highly porous and comprise needles (2−3 μm in thickness) and bushy structures. Depositions in EC/DEC (Figure 1a,d) formed sodium clusters stemming from thin, needlelike roots. The fragility of these dendrites is illustrated in Figure S3a,b were gas bubbles caused detachment of the sodium deposits at 1 mA cm^{-2}. The dendrites formed in PC/FEC (Figure 1b,e) grew more globular in appearance and had reduced needle deposits. Additionally, the color of these dendrites is closer to that of the sodium substrate compared to the EC/DEC dendrites, perhaps due to differing SEIs.[21] In the FEC/DEC electrolyte (Figure 1c) at 1 mA cm^{-2}, a highly porous deposit was produced; at 5 mA cm^{-2}

DOI: 10.1021/acsenergylett.7b00500
ACS Energy Lett. 2017, 2, 2051−2057

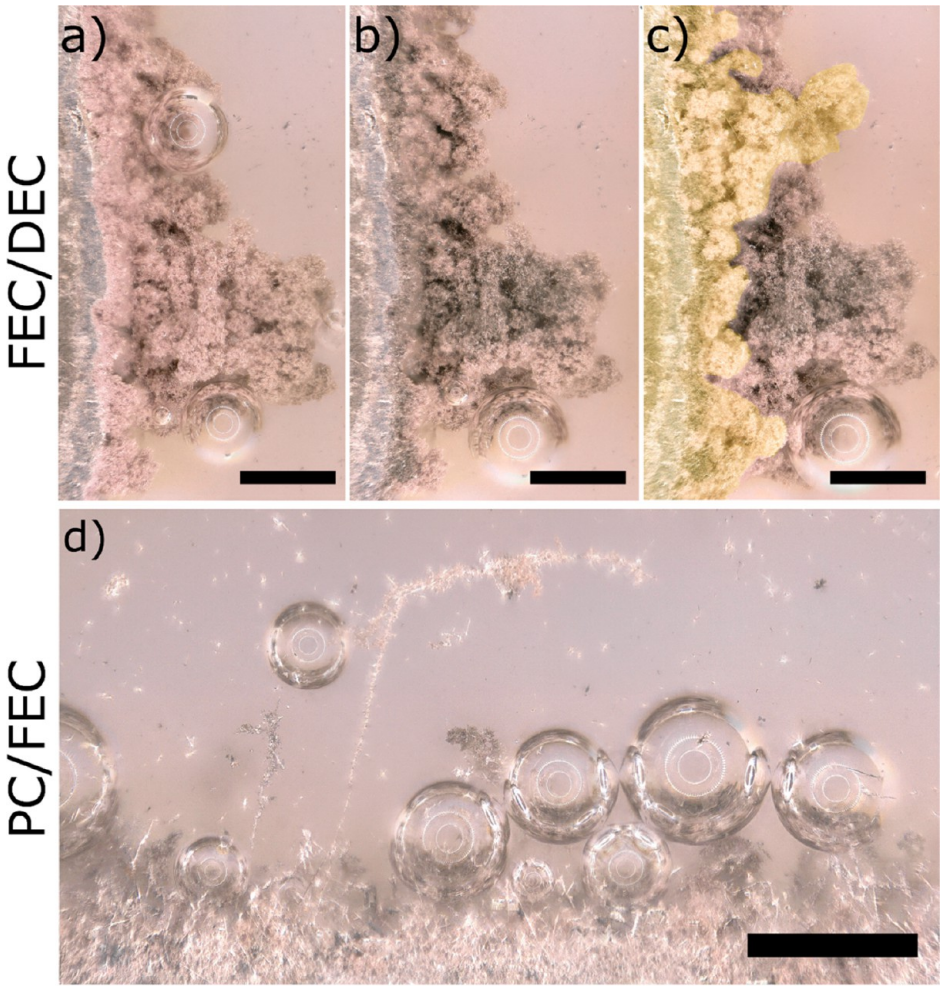

Figure 2. Sodium deposits and gassing in FEC/DEC (a–c) and PC/FEC (d). First deposition half cycle (a); first dissolution, i.e. discharge, half-cycle (b); second deposition half cycle (c) where the sodium layer growing under the first is artificially highlighted in yellow. Needles and gassing in the second deposition half-cycle in PC/FEC (d). 2 mAh cm^{-2}; 2.5 mA cm^{-2}; 500 μm scale bar.

(Figure 1f) the deposit was still porous, but less so than the 1 mA cm^{-2} deposition.

For all the electrolytes, the fast charge rate caused an increase in gas evolution due to increased SEI formation at higher overpotentials[22] and an increase in nucleation density. The typical exacerbation of porosity upon increasing the current density and concentration polarization was not observed.[12,23−25] The denser depositions are due to increased formation of sodium nuclei at faster charge rates.[26] An example of electrodepositions at a very slow rate (0.25 mA cm^{-2}) demonstrating small nucleation density is shown in Figure S5. Overall, the order of increasing deposition thickness at 5 mA cm^{-2} was PC/FEC < FEC/DEC < EC/DEC; at 1 mA cm^{-2} it was PC/FEC < FEC/DEC, the sodium in the EC/DEC at 1 mA cm^{-2} being so fragile that it cannot be compared here. Figure S4 illustrates the growth of the sodium anode deposition layer for the FEC/DEC and PC/FEC electrolytes (at 5 mA cm^{-2} passing 1 mAh cm^{-2} of charge) as a function of cycle number. For both electrolytes, the largest change in dendritic growths occurred in the first and second cycles. The mean heights of the dendrites in the first depositions (determined by the integrated average of the projected deposition area) were 120 and 104 μm for the FEC/DEC and PC/FEC, respectively. In the second cycle, the mean dendritic heights doubled for the FEC/DEC and PC/FEC (267 and 192 μm, respectively). Finally, in the third and fourth cycle the deposition heights changed less than 30% each time for both electrolytes.

Figure 2 shows images from Supporting Information Videos 2 and 3 for FEC/DEC (a–c) and PC/FEC (d). Images involving EC/DEC (Video 1) as the electrolyte solvent are not shown, because gas evolution became too problematic. It is evident from the Supporting Information videos that the rate of gas evolution decreased in the following order: EC/DEC > PC/FEC > FEC/DEC. Note that the second deposition on the highly porous deposit with FEC/DEC as the electrolyte solvent (Figure 2c) occurred under, not on, the sodium deposited in the first cycle. This indicates that the previously deposited dendrites made poor electrical contact with the electrode (dead sodium). Similar deposition behavior on lithium was observed by Steiger et al.[11] As the electrode was stripped in the FEC/DEC, the sodium dendrites changed into a darker shade of gray (Figure 2a,b). Despite passing 2 mAh cm^{-2} in both the charge and discharge cycles (Videos 2 and 3), the deposition layers in the PC/FEC and FEC/DEC electrolytes showed minimal changes in size.

In the second charge/discharge cycle in PC/FEC (Figure 2d) the sodium layer was more compact than that in FEC/DEC. The deposition appeared to first form needlelike dendrites, and as more charge was passed, the formation of three-dimensional structures began to develop. Occasionally, as

DOI: 10.1021/acsenergylett.7b00500
ACS Energy Lett. 2017, 2, 2051−2057

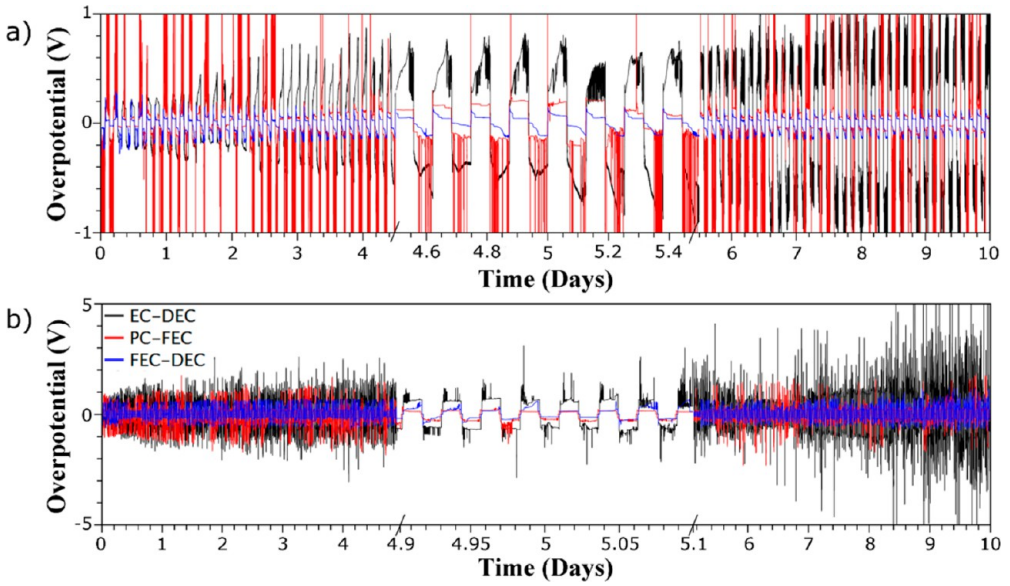

Figure 3. Time dependence of the potential of symmetrical sodium electrode coin cells passing 1.5 mAh cm^{-2} of charge at 1 mA cm^{-2} (a) and 5 mA cm^{-2} (b). Black, red, and blue curves are EC/DEC, PC/FEC, and FEC/DEC, respectively.

seen in Figure 2d, a very long, thick (6−10 μm) dendrite appears; it grows, as observed by Steiger's study of lithium dendrites, from the base and kinks.[25] As the growing dendrite in Figure 2d approached the Na foil counter electrode, the higher Na^+ flux resulted in growth of many branched structures (Video 3). This erratic dendritic growth is attributed to a diminishing electrochemically active area caused by the ionically insulating gas bubbles.[12] The deposition layer is thinner, i.e., it is denser, in the second deposition half cycle than in the first, both in FEC/DEC and PC/FEC. The densification is attributed to residual sodium nuclei from the first cycle, which in combination with nucleation in the second, increased the number density of nucleation sites. The Tarascon group observed a similar trend for lithium and identified pits as nucleation sites.[27] Dendrites nucleating in sodium pits can be seen in Video 5.

After the optical cell with the sodium electrodes and electrolyte is assembled (with no applied potential), gradual gas evolution occurs for all solvents but eventually ceases if FEC is present in the electrolyte. Rapid gas evolution occurs in the EC/DEC and PC/FEC electrolyte when the optical cell is cycled because of a slow passivation of the sodium surface as new structures form, requiring the formation of new SEI. The gas bubbles in the PC/FEC and EC/DEC often dislodged fragile sodium fragments from the deposits (Video 4). In the FEC/DEC electrolyte, gas evolution was mitigated (Video 2) because of the abundance of FEC in this electrolyte. Dugas et al. found similar results in their gas chromatograph studies of FEC as an electrolyte additive for SIBs.[1]

As seen in Figure 3a,b, the time dependence of the voltage of the galvanostatically cycled cells with different electrolyte solvents varied both in the symmetrical baseline voltage excursions and in the frequency of spikes. At 1 mA cm^{-2} the baseline excursions for FEC/DEC were frequent, but they began to disappear after the second day indicating that large gas bubbles or other causes of electrical discontinuity had been inhibited. At 1 mA cm^{-2} the symmetrical baseline excursions were the largest in magnitude for the PC/FEC electrolyte and persisted throughout the entire cycling test for the cell. Baseline excursions were also seen through the entire cycling test of the EC/DEC, increasing in magnitude over time. At the faster charge rate (Figure 3b), baseline excursions persist throughout testing for all the electrolyte compositions but are much more frequent and higher in magnitude for the EC/DEC electrolyte. Additionally, voltage spike magnitudes increased over time in the EC/DEC electrolyte.

Voltage spikes can occur because of either gas bubbles[28,29] or dead sodium[30,31] decreasing the electrochemically active electrode surface. Thus, the dendrites formed in the FEC/DEC (Figure 1a,d) greatly reduce electrolyte consumption and the formation of dead sodium. Song et al. saw the same trend in their study of FEC on symmetrical lithium cells.[2] It is interesting to note that PC/FEC voltage excursions were the largest in magnitude at 1 mA cm^{-2} but not so at 5 mA cm^{-2}. We speculate that the larger voltage excursions observed in the PC/FEC solvent at 1 mA cm^{-2} compared to 5 mA cm^{-2} are related to the decreased nucleation sites formed at smaller current densities. Thus, passing the same total amount of charge with a current density of 1 mA cm^{-2} results in fewer, larger dendritic structures compared to depositions at 5 mA cm^{-2} which form more numerous but relatively smaller structures. For the case of 1 mA cm^{-2}, detachment of a dendrite will therefore result in a larger loss of electrochemically active surface area compared to the case of 5 mA cm^{-2}. This leads to a sudden increase in voltage to supply the constant current imposed and results in high-magnitude voltage excursions. Additionally, on lithium electrodepositions the frequency of electrical disconnects (i.e., dendrite detachment) from the metal anode can be reduced by discharging (stripping) at a faster rate.[32]

Figure 4a shows Nyquist plots of all the electrolytes prior to cycling and after a 12 h rest. The FEC/DEC and PC/FEC electrolytes showed similar cell impedance while the EC/DEC electrolyte demonstrated the highest impedance. Fitting the equivalent circuit shown in Figure 4a, the summed resistances (R2, R3, and R4) were 6.3, 3.4, and 3.6 kΩ for EC/DEC, PC/FEC, and FEC/DEC, respectively. The equivalent circuit model was adopted from Aurbach.[33] In this model, the parallel

DOI: 10.1021/acsenergylett.7b00500
ACS Energy Lett. 2017, 2, 2051−2057

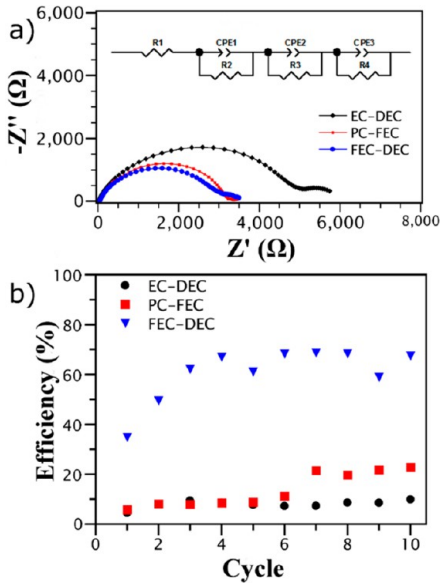

Figure 4. Nyquist plots with inset equivalent circuit (a). Cycle number dependence of the percentage of the retained Coulombic efficiency (b); 1 mAh cm^{-2} per cycle at 1 mA cm^{-2}.

resistor and constant phase element components represent the organic/inorganic interphases found in the SEI.[34] Though the cell impedances were similar for the FEC/DEC and PC/FEC electrolytes, the baseline overpotentials can vary significantly during some cycles. We attribute this discrepancy to the formation of gas bubbles and the nature of the high surface area sodium deposition behavior with the FEC/DEC electrolyte (Figure 1c) compared to PC/FEC (Figure 1b) at slow rates. Both of these variables will affect the electrochemically active area of the sodium anodes which is reflected by the overpotential.

The loss of electrically connected sodium deposits was monitored by measuring the Coulombic efficiency in coin cells with aluminum substrates and sodium counter/reference electrodes at 1 mA cm^{-2} (Figure 4b). After the first 10 cycles, the Coulombic efficiency was highest in the FEC/DEC electrolyte, but it was still only about 70%; in the PC/FEC it was merely about 20%, and it was even less, only about 10%, in the EC/DEC. Despite leaving an apparently large amount of dead sodium upon cycling (Figure 2a–c), cycling efficiencies where high (60–70%) for the FEC/DEC. This can be explained by the effect of stack pressure on cycling efficiencies in coin cells. The compact nature of the cells confines dendrites to the sodium substrate's surface, which helps the dendrites stay electronically connected and reduces electrolyte consumption.[27]

Figure 5 shows time of flight secondary-ion mass spectrometry, a highly elemental and surface sensitive technique,[35] depth profiling of the SEI formed in the EC/DEC and FEC/DEC electrolytes. Here, increasing sputtering time corresponds to increasing film depth. The profiles indicate a mixture of inorganic and organic decomposition species situated at similar depths while forming the SEI. There are four secondary ionic fragments of interest denoting different SEI species: NaF_2^- from the PF_6^- and FEC, the PO^- from salt-reacted PF_6^- via $P_xO_yF_z$, and CO_3^- from Na_2CO_3 and other carbonate species (such as disodium ethylenedicarbonate) derived of FEC and DEC.[6,36−38] The C_2^- curve is a proxy for organic SEI species such as Na-alkoxides or polyolefins.[6,39] A high and flat C_2^- plateau is observed consistent with a dense organic polymer layer; the cause of the plateau in EC/DEC is not sensor saturation, but uniformity of the composition of the deposited organic polymer layer. The values of the full width at half maximum for all ionic fragments in the FEC/DEC are higher than those of the EC/DEC, which implies that the FEC/DEC derived SEI is thicker than the EC/DEC SEI. This may be because the sodium anode reacts indefinitely with the EC/DEC electrolyte and consequently forms an incomplete SEI. The indefinite corrosion of sodium in EC/DEC may also explain why the impedance was larger for EC/DEC (Figure 3a) despite having a thinner SEI; the resulting gas evolution from the electrolyte degradation should affect the EIS measurement by blocking the electrode surface area. Though the SEI formed in the FEC/DEC is thicker than that in the EC/DEC, the SEI structure is essentially unaffected by the fluorination of EC in regards to where the maxima occur (Figure 4b).[37]

The Na-derived SEIs are more unstable than their Li analogs because of the increased solubility of Na decomposition products.[40] The use of FEC/DEC as a solvent serves to form an SEI richer in NaF than the EC/DEC electrolyte. NaF makes

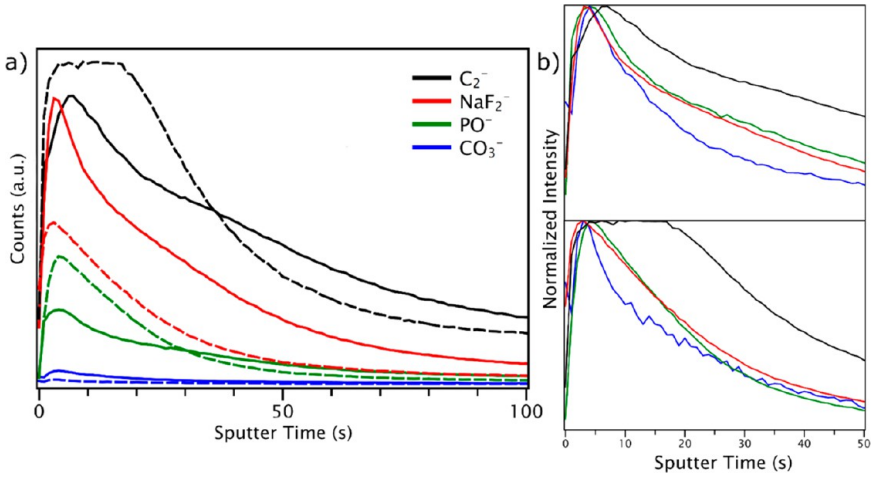

Figure 5. ToF-SIMS depth profiles of sodium soaked in 1 M $NaPF_6$ EC/DEC (dashed lines) and FEC/DEC (solid lines) for 12 h (a). The normalized intensities for FEC/DEC (top) and EC/DEC (bottom) are shown in panel b.

DOI: 10.1021/acsenergylett.7b00500
ACS Energy Lett. 2017, 2, 2051−2057

for an exceptional SEI compound due its electrical insulating properties and poor solubility.[6,40] The passivating nature of NaF may also explain the lowered PO^- counts in the FEC/DEC electrolyte; a weaker PO^- signal implies less PF_6^- salt reacted. Interactions of the LiF with other SEI components have been shown to hold lithium SEIs together; this "glue" effect may be occurring here as well.[41] The weak CO_3^- signal from the EC/DEC compared to the FEC/DEC implies that the organic polymer layer was deplete of carbonate-containing species and was largely composed of polyolefins. Most importantly, there is less organic matter when the EC is replaced by FEC because inorganics tend to be more stable in the SEI.[10,8]

In conclusion, deposition of sodium in standard organic solvents resulted in highly porous electrodeposits. The sodium dendrites formed in the EC/DEC and PC/FEC solvents were easily expelled into the electrolyte as gas generation occurred. Despite producing the most porous depositions, gas evolution and sodium loss could be greatly decreased when the FEC was used as a cosolvent. In this FEC/DEC electrolyte, cycling efficiency and performance were improved. ToF-SIMS depth profiling revealed that FEC created an SEI on Na that was richer in NaF compared to EC; this NaF rich SEI resulted in lowered levels of organic and PF_6^- reduction products. The results shown here raise questions about the use of Na as a counter/reference electrode in SIB research when standard solvents are utilized. The ToF-SIMS data suggests that doping the surface of Na with fluorine-rich compounds may lead to stable sodium depositions with cycling efficiencies that are higher than those achieved here.

■ ASSOCIATED CONTENT

Supporting Information

The Supporting Information is available free of charge on the ACS Publications website at DOI: 10.1021/acsenergylett.7b00500.

Experimental procedures and optical-cell schematics (PDF)
Video 1, EC/DEC (MPG)
Video 2, FEC/DEC (MPG)
Video 3, PC/FEC (MPG)
Video 4, gas bubbles dislodging fragile sodium fragments from the deposits (MPG)
Video 5, dendrites nucleating in sodium pits (MPG)

■ AUTHOR INFORMATION

Corresponding Author

*E-mail: mullins@che.utexas.edu.

ORCID

Andrei Dolocan: 0000-0001-5653-0439
C. Buddie Mullins: 0000-0003-1030-4801

Notes

The authors declare no competing financial interest.

■ ACKNOWLEDGMENTS

Welch Foundation Grants F-1131 (AH) and F-1436 (CBM) as well as National Science Foundation Grant CBET-1603491 generously supported this study. The National Science Foundation Major Research Instrumentation program (DME-0923096) funded the ToF-SIMS at UT-Austin. The authors also thank Celgard Corp. for their provision of separators and Solvay Fluor for their donation of fluoroethylene carbonate. We also thank Dr. Krishnaswamy Ravi-Chandar for use of his Keyence VHX-5000 digital microscope.

■ REFERENCES

(1) Dugas, R.; Ponrouch, A.; Gachot, G.; David, R.; Palacin, M. R.; Tarascon, J. M. Na Reactivity Toward Carbonate-Based Electrolytes: The Effect of FEC as Additive. *J. Electrochem. Soc.* **2016**, *163*, A2333−A2339.

(2) Song, J.-H.; Yeon, J.-T.; Jang, J.-Y.; Han, J.-G.; Lee, S.-M.; Choi, N.-S. Effect of Fluoroethylene Carbonate on Electrochemical Performances of Lithium Electrodes and Lithium-Sulfur Batteries. *J. Electrochem. Soc.* **2013**, *160*, A873−A881.

(3) Yui, Y.; Hayashi, M.; Nakamura, J. In situ Microscopic Observation of Sodium Deposition/Dissolution on Sodium Electrode. *Sci. Rep.* **2016**, *6*, 22406.

(4) Cheng, X.-B.; Zhang, R.; Zhao, C.-Z.; Wei, F.; Zhang, J.-G.; Zhang, Q. A Review of Solid Electrolyte Interphases on Lithium Metal Anode. *Adv. Sci.* **2016**, *3*, 1500213.

(5) Peled, E. The Electrochemical Behavior of Alkali and Alkaline Earth Metals in Nonaqueous Battery Systems—The Solid Electrolyte Interphase Model. *J. Electrochem. Soc.* **1979**, *126*, 2047−2051.

(6) Kumar, H.; Detsi, E.; Abraham, D. P.; Shenoy, V. B. Fundamental Mechanisms of Solvent Decomposition Involved in Solid-Electrolyte Interphase Formation in Sodium Ion Batteries. *Chem. Mater.* **2016**, *28*, 8930−8941.

(7) Morigaki, K.; Ohta, A. Analysis of the Surface of Lithium in Organic Electrolyte by Atomic Force Microscopy, Fourier Transform Infrared Spectroscopy and Scanning Auger Electron Microscopy. *J. Power Sources* **1998**, *76*, 159−166.

(8) Sacci, R. L.; Black, J. M.; Balke, N.; Dudney, N. J.; More, K. L.; Unocic, R. R. Nanoscale Imaging of Fundamental Li Battery Chemistry: Solid-Electrolyte Interphase Formation and Preferential Growth of Lithium Metal Nanoclusters. *Nano Lett.* **2015**, *15*, 2011−2018.

(9) Seh, Z. W.; Sun, J.; Sun, Y.; Cui, Y. A Highly Reversible Room-Temperature Sodium Metal Anode. *ACS Cent. Sci.* **2015**, *1*, 449−455.

(10) Iermakova, D. I.; Dugas, R.; Palacín, M. R.; Ponrouch, A. On the Comparative Stability of Li and Na Metal Anode Interfaces in Conventional Alkyl Carbonate Electrolytes. *J. Electrochem. Soc.* **2015**, *162*, A7060−A7066.

(11) Steiger, J.; Kramer, D.; Mönig, R. Microscopic Observations of the Formation, Growth and Shrinkage of Lithium Moss During Electrodeposition and Dissolution. *Electrochim. Acta* **2014**, *136*, 529−536.

(12) Bai, P.; Li, J.; Brushett, F. R.; Bazant, M. Z. Transition of Lithium Growth Mechanisms in Liquid Electrolytes. *Energy Environ. Sci.* **2016**, *9*, 3221−3229.

(13) Wood, K. N.; Kazyak, E.; Chadwick, A. F.; Chen, K.-H.; Zhang, J.-G.; Thornton, K.; Dasgupta, N. P. Dendrites and Pits: Untangling the Complex Behavior of Lithium Metal Anodes through Operando Video Microscopy. *ACS Cent. Sci.* **2016**, *2*, 790−801.

(14) Wu, H.; Zhuo, D.; Kong, D.; Cui, Y. Improving Battery Safety by Early Detection of Internal Shorting with a Bifunctional Separator. *Nat. Commun.* **2014**, *5*, 5193.

(15) Love, C. T.; Baturina, O. A.; Swider-Lyons, K. E. Observation of Lithium Dendrites at Ambient Temperature and Below. *ECS Electrochem. Lett.* **2015**, *4*, A24−A27.

(16) Wei, S.; Choudhury, S.; Xu, J.; Nath, P.; Tu, Z.; Archer, L. A. Highly Stable Sodium Batteries Enabled by Functional Ionic Polymer Membranes. *Adv. Mater.* **2017**, *29*, 1605512.

(17) Wood, S. M.; Pham, C. H.; Rodriguez, R.; Nathan, S. S.; Dolocan, A. D.; Celio, H.; de Souza, J. P.; Klavetter, K. C.; Heller, A.; Mullins, C. B. K+ Reduces Lithium Dendrite Growth by Forming a Thin, Less-Resistive Solid Electrolyte Interphase. *ACS Energy Lett.* **2016**, *1*, 414−419.

(18) Komaba, S.; Ishikawa, T.; Yabuuchi, N.; Murata, W.; Ito, A.; Ohsawa, Y. Fluorinated Ethylene Carbonate as Electrolyte Additive for

DOI: 10.1021/acsenergylett.7b00500
ACS Energy Lett. 2017, 2, 2051−2057

Rechargeable Na Batteries. *ACS Appl. Mater. Interfaces* **2011**, *3*, 4165−4168.
(19) Bhide, A.; Hofmann, J.; Katharina Dürr, A.; Janek, J.; Adelhelm, P. Electrochemical Stability of Non-Aqueous Electrolytes for Sodium-Ion Batteries and Their Compatibility with $Na_{0.7}CoO_2$. *Phys. Chem. Chem. Phys.* **2014**, *16*, 1987−1998.
(20) Ponrouch, A.; Monti, D.; Boschin, A.; Steen, B.; Johansson, P.; Palacín, M. R. Non-aqueous Electrolytes for Sodium-Ion Batteries. *J. Mater. Chem. A* **2015**, *3*, 22−42.
(21) Qian, J.; Henderson, W. A.; Xu, W.; Bhattacharya, P.; Engelhard, M.; Borodin, O.; Zhang, J.-G. High Rate and Stable Cycling of Lithium Metal Anode. *Nat. Commun.* **2015**, *6*, 6362.
(22) Lu, P.; Li, C.; Schneider, E. W.; Harris, S. J. Chemistry, Impedance, and Morphology Evolution in Solid Electrolyte Interphase Films during Formation in Lithium Ion Batteries. *J. Phys. Chem. C* **2014**, *118*, 896−903.
(23) Aurbach, D.; Zinigrad, E.; Cohen, Y.; Teller, H. A Short Review of Failure Mechanisms of Lithium Metal and Lithiated Graphite Anodes in Liquid Electrolyte Solutions. *Solid State Ionics* **2002**, *148*, 405−416.
(24) Bard, A. J.; Faulkner, L. R. *Electrochemical Methods: Fundamentals and Applications*, 2nd ed.; Wiley: New York, 2001.
(25) Steiger, J.; Kramer, D.; Mönig, R. Mechanisms of Dendritic Growth Investigated by In Situ Light Microscopy During Electrodeposition and Dissolution of Lithium. *J. Power Sources* **2014**, *261*, 112−119.
(26) Pei, A.; Zheng, G.; Shi, F.; Li, Y.; Cui, Y. Nanoscale Nucleation and Growth of Electrodeposited Lithium Metal. *Nano Lett.* **2017**, *17*, 1132−1139.
(27) Gireaud, L.; Grugeon, S.; Laruelle, S.; Yrieix, B.; Tarascon, J.-M. Lithium Metal Stripping/Plating Mechanisms Studies: A Metallurgical Approach. *Electrochem. Commun.* **2006**, *8*, 1639−1649.
(28) Moshkovich, M.; Cojocaru, M.; Gottlieb, H. E.; Aurbach, D. The Study of the Anodic Stability of Alkyl Carbonate Solutions by In Situ FTIR Spectroscopy, EQCM, NMR and MS. *J. Electroanal. Chem.* **2001**, *497*, 84−96.
(29) Gabrielli, C.; Huet, F.; Keddam, M.; Macias, A.; Sahar, A. Potential Drops Due to an Attached Bubble on a Gas-Evolving Electrode. *J. Appl. Electrochem.* **1989**, *19*, 617−629.
(30) Howlett, P. C.; MacFarlane, D. R.; Hollenkamp, A. F. A Sealed Optical Cell for the Study of Lithium-Electrode|Electrolyte Interfaces. *J. Power Sources* **2003**, *114*, 277−284.
(31) Bieker, G.; Winter, M.; Bieker, P. Electrochemical In Situ Investigations of SEI and Dendrite Formation on the Lithium Metal Anode. *Phys. Chem. Chem. Phys.* **2015**, *17*, 8670−8679.
(32) Yamaki, J.; Tobishima, S.; Hayashi, K.; Saito, K.; Nemoto, Y.; Arakawa, M. A Consideration of the Morphology of Electrochemically Deposited Lithium in an Organic Electrolyte. *J. Power Sources* **1998**, *74*, 219−227.
(33) Aurbach, D. Review of Selected Electrode−Solution Interactions Which Determine the Performance of Li and Li Ion Batteries. *J. Power Sources* **2000**, *89*, 206−218.
(34) Aurbach, D.; Zaban, A. Impedance Spectroscope of Lithium Electrodes. *J. Electroanal. Chem.* **1994**, *367*, 15−25.
(35) Chou, H.; Ismach, A.; Ghosh, R.; Ruoff, R. S.; Dolocan, A. Revealing the Planar Chemistry of Two-Dimensional Heterostructures at the Atomic Level. *Nat. Commun.* **2015**, *6*, 7482.
(36) Jorn, R.; Kumar, R.; Abraham, D. P.; Voth, G. A. Atomistic Modeling of the Electrode−Electrolyte Interface in Li-Ion Energy Storage Systems: Electrolyte Structuring. *J. Phys. Chem. C* **2013**, *117*, 3747−3761.
(37) Schroder, K.; Alvarado, J.; Yersak, T. A.; Li, J.; Dudney, N.; Webb, L. J.; Meng, Y. S.; Stevenson, K. J. The Effect of Fluoroethylene Carbonate as an Additive on the Solid Electrolyte Interphase on Silicon Lithium-Ion Electrodes. *Chem. Mater.* **2015**, *27*, 5531−5542.
(38) Liu, Q.; Mu, D.; Wu, B.; Wang, L.; Gai, L.; Wu, F. Density Functional Theory Research into the Reduction Mechanism for the Solvent/Additive in a Sodium-Ion Battery. *ChemSusChem* **2017**, *10*, 786−796.
(39) Peled, E.; Golodnitsky, D.; Ardel, G. Advanced Model for Solid Electrolyte Interphase Electrodes in Liquid and Polymer Electrolytes. *J. Electrochem. Soc.* **1997**, *144*, L208−L210.
(40) Mogensen, R.; Brandell, D.; Younesi, R. Solubility of the Solid Electrolyte Interphase (SEI) in Sodium Ion Batteries. *ACS Energy Lett.* **2016**, *1*, 1173−1178.
(41) Okuno, Y.; Ushirogata, K.; Sodeyama, K.; Tateyama, Y. Decomposition of the Fluoroethylene Carbonate Additive and the Glue Effect of Lithium Fluoride Products for the Solid Electrolyte Interphase: An Ab Initio Study. *Phys. Chem. Chem. Phys.* **2016**, *18*, 8643−8653.

DOI: 10.1021/acsenergylett.7b00500
ACS Energy Lett. 2017, 2, 2051−2057